Failure Mode and Failure Strengths for Wall Thinning Straight Pipes and Elbows Subjected to Seismic Loading

Kunio Hasegawa[1]
Nuclear System Division,
Hitachi, Ltd.,
Saiwai-cho 3-1-1, Hitachi-shi,
317-8511 Ibaraki-ken, Japan
e-mail: hasegawa-kunio@jnes.go.jp

Katsumasa Miyazaki
Hitachi Research Laboratory,
Hitachi, Ltd.,
Saiwai-cho 3-1-1, Hitachi-shi,
317-8511 Ibaraki-ken, Japan
e-mail: katsumasa.miyazaki.xs@hitachi.com

Izumi Nakamura
National Research Institute for Earth Science and Disaster Prevention,
Miki-shi, Hyogo-ken 673-0515, Japan
e-mail: izumi@bosai.go.jp

It is important to assess the failure strengths for pipes with wall thinning to maintain the integrity of the piping systems and to make codification of allowable wall thinning. Full-scale fracture experiments on cyclic loading under constant internal pressure were performed for 4 in. *diameter straight pipes and* 8 in. *diameter elbow pipes at ambient temperature. The experiments were low cycle fatigue under displacement controlled conditions. It is shown that a dominant failure mode under cyclic loading for straight pipes and elbows is crack initiation/growth accompanying swelling by ratchet or buckling with crack initiation. When the thinning depth is deep, the failure mode is burst and crack growth with ratchet swelling. In addition, failure strengths were compared with the design fatigue curve of the ASME Code Sec. III. It is shown that pipes with wall thinning less than 50% of wall thickness have sufficient margins against a seismic event of the safety shutdown earthquake.* [DOI: 10.1115/1.2826425]

Introduction

Carbon steel is one of the principal structural materials being used extensively in piping systems in nuclear power plants. High temperature water or steam with high pressure flows at high velocities through these pipes. Erosion corrosion has caused wall thinning in high energy carbon steel piping. After severe erosion corrosion wall thinning led to failures of carbon steel piping at Surry Unit 2 in 1986 and at Mihama Unit 3 Nuclear Plants in 2004, wall thinning became more important aging degradations for power plants. Programs during in-service inspection were strengthened during periodic examinations, and a management guideline on wall thinning for nuclear and thermal power plants will soon be published by a special task group of Japanese Society of Mechanical Engineers (JSME) [1].

On the other hand, it is important to assess failure strengths for pipes with wall thinning to maintain the integrity of piping systems and to make codification of allowable wall thinning. Burst and monotonic bending tests with internal pressure were performed on 6 in. diameter carbon steel pipes with wall thinning by Japan Atomic Energy Research Institute (JAERI), currently Japan Atomic Energy Agency [2]. Quasistatic bending tests without internal pressure were conducted on 4 in. diameter straight pipes with wall thinning at ambient temperature [3,4]. Low cycle fatigue tests were performed on 4 in. diameter straight pipes with allowable wall thinning depths [5]. In addition, numerical analyses were conducted to estimate deformation behavior and failure stresses [6,7]. From these experimental and analytical results, it was shown that failure behaviors for wall thinning were classified into three types at maximum loads; deformation of ovalization, local buckling, and crack initiation. In addition, monotonic fracture load was known to be high when the thinned thickness of a pipe was the minimum required wall thickness defined in terms of design pressure, and failure assessment procedures derived from the monotonic failure load tests are discussed to use allowable stress for wall thinning pipes at the American Society of Mechanical Engineers (ASME) Code Sec. XI working group on pipe flaw evaluation [8]. However, experiments of cyclic loading together with constant internal pressure were not prevalent for wall thinning pipes [9], and these experimental data will be useful for assessment of a seismic event such as a safety shutdown earthquake (SSE).

This study was undertaken in order to clarify the fracture behaviors of wall thinning pipes subjected to cyclic bending stress under constant internal pressure. In addition, cyclic failure strengths of carbon steel pipes containing wall thinning were compared with the design fatigue curves in Sec. III of ASME Code and discussed on the integrity against SSE.

Experimental Procedures

Pipe Specimens. The materials used in this experiments were carbon steel pipes, JIS STS 410 (Japanese Industrial Standards: carbon steel pipes for high pressure service), which corresponds to ASTM A333 Gr. 6. The material is commonly used in Class 1 coolant piping systems in nuclear power plants in Japan. Mechanical properties and chemical composition are shown in Table 1.

Two kinds full-scale pipe experiments were conducted on straight and elbow pipes using a shaking table [9]. For a full-scale straight pipe specimen, a four-point bending test was performed on a 4 in. diameter schedule 80 pipe with 360 deg wall thinning. The nominal outer diameter was 114.3 mm, and the nominal wall thickness was 8.6 mm. The wall thinning was machined by cutting to simulate erosion/corrosion on the inside of the straight pipe. The pipe configuration and the wall thinning are shown in Fig. 1. The angle of the thinning was 360 deg, and the depth of the thinning was $d/t=25\%$, 50%, 60%, and 75%, where d and t are the nominal wall thinning depth and wall thickness, respectively. The wall thinning depth is the depth of metal loss in the thickness direction. The axial length of the wall thinning of constant depth was 75 mm, and the lengths of both sides to the nominal wall thickness were 62.5 mm. The total axial length of the wall thinning was 200 mm.

For a full-scale elbow specimen, a 90 deg forged elbow pipe specimen was used. The diameter of the elbow was 8 in. schedule 80 elbow with bent radius of 304.8 mm. The nominal outer diam-

[1]Present address: Japan Nuclear Energy Safety Organization.

Contributed by the Pressure Vessel and Piping Division of ASME for publication in the JOURNAL OF PRESSURE VESSEL TECHNOLOGY. Manuscript received February 9, 2006; final manuscript received January 8, 2007; published online January 17, 2008. Review conducted by William Koves. Paper presented at the 2005 ASME Pressure Vessels and Piping Conference (PVP2005), Denver, CO, July 17–21, 2005.

Table 1 Mechanical properties and chemical composition of pipe (Note σ_y: yield stress, σ_U: UTS)

Material	Specimen	Mechanical		Chemical composition (wt %)				
		σ_y (MPa)	σ_U (MPa)	C	Si	Mn	P	S
STS 410	EC02	345	509	0.21	0.18	0.73	0.01	0.006
	EC05, 06, 07, 08, 09	312	470	0.20	0.24	0.43	0.02	0.002
	ELB01, 02, 03, 04	362	553	0.17	0.20	0.50	0.01	0.002
	ELB05, ELBI-01, ELBO-01, 02, ELBM-01	351	506	0.19	0.25	0.82	0.02	0.004

eter of the elbow was 216.3 mm, and the nominal wall thickness was 12.7 mm. The ends of the elbow were welded with 8 in. diameter schedule 80 straight pipes with 1025.2 mm lengths. The total length of the straight pipe, elbow, and flange was 1380 mm, as shown in Fig. 2 (1). Figure 2 (3) shows the geometries of the elbow specimens with wall thinning. There are four types of elbow specimens: no defect, 50% full circumferential, 50% and 70% partial wall thinning at the flank.

Loading Conditions. A cyclic four-point bending load was conducted for the straight pipe specimens with a shaking table at ambient temperature. Figure 3 is a schematic drawing illustrating the four-point bending frame used for these experiments. The major and minor spans were 800 mm and 2400 mm, respectively. The specimens on the shaking table were subjected to bending load under displacement controlled conditions with or without internal pressure [9].

In the case of full-scale elbow specimens, cyclic loading under displacement controlled conditions was performed under the conditions of pin-pin or pin-fixed supports. In addition, there are three loading directions: in plane, out of plane, and a combination of in and out of plane. Specimen setup of pin-pin support with in-plane direction is shown in Fig. 4(*a*). Figure 4(*b*) shows the test apparatus of pin-fixed support with in plane, out of plane, and combination of in and out of plane. All specimens were loaded under displacement controlled conditions with internal pressure at ambient temperature [9].

The experiments were conducted by first pressurizing the pipe specimens to the pressure of 11 MPa for a straight pipe and to 10 MPa for an elbow, using water. Then, a bending load was applied by the shaking table until failure or leakage occurred. These internal pressures for specimens were slightly higher than those of service pressure of 8 MPa for schedule 80 pipes. Hoop stresses due to internal pressure for straight pipe and elbow are 68 MPa and 80 MPa, respectively.

The patterns of the input displacements for straight pipe and elbow pipe specimens are shown in Fig. 5. The displacement input is a sinusoidal wave. Figure 5 (1) is a wave for straight pipe. The frequency of the wave was 1 Hz, and the number of the steady amplitude of one block is 26 cycles. The input displacement of sinusoidal waves for elbow specimens was 0.2 Hz, shown in Figs. 5 (2) and 5 (3). The number of cycles in one block of Fig. 5 (2) is 5 cycles and that of Fig. 5 (3) is 20 cycles. The input data of applied displacements for each straight pipe and elbow are shown in Tables 2 and 3.

Results of Experiments

Failure Modes. The failure mode of local wall thinning pipe with increasing internal pressure is a burst accompanying bulging at the wall thinning area [2]. Failure modes of wall thinning pipes subjected to monotonic bending moment without internal pressure are a little complicated, reported to be classified into three types: ovalization, local buckling, and crack initiation/growth at the maximum moments [3]. When a wall thinning area in a pipe is subjected to tensile stress, ovalization occurs at the thinning section of the wall thinning pipe, or crack initiates and grows at the

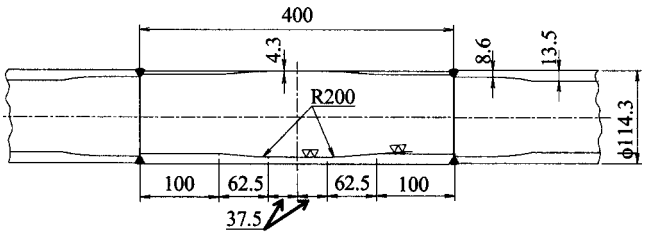

(1) 50% thinned specimen (EC02, 05, 06)

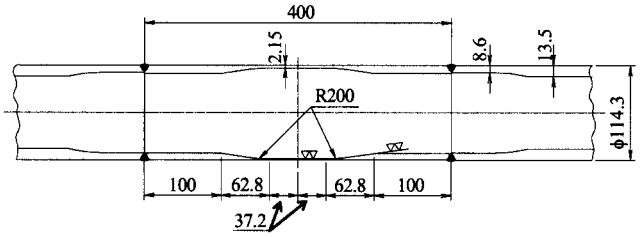

(2) 75% thinned specimen (EC07)

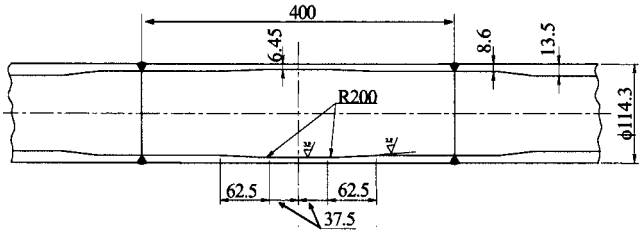

(3) 25% thinned specimen (EC08)

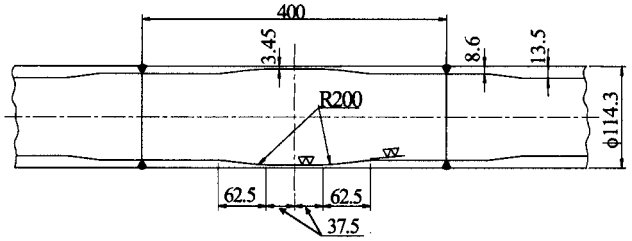

(4) 60% thinned specimen (EC09)

Fig. 1 Straight pipe specimens with full circumferential wall thinning. (1) 50% thinned specimen (EC02, 05, 06). (2) 75% thinned specimen (EC07). (3) 25% thinned specimen (EC08). (4) 60% thinned specimen (EC09).

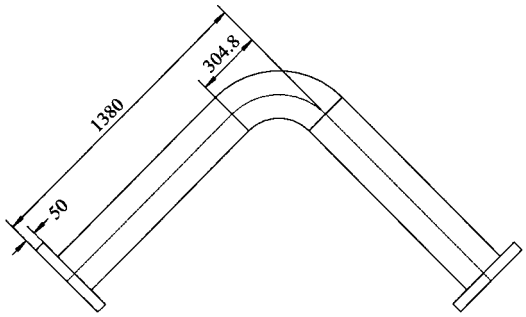

(1) Elbow specimen

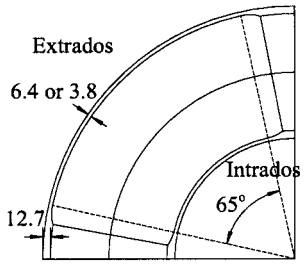

(2) Longitudinal section

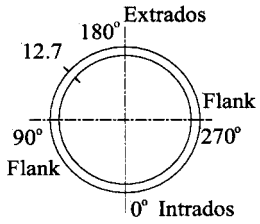

(a) No defect

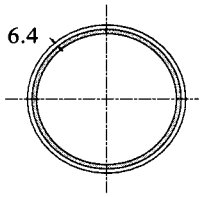

(b) 50% full defect

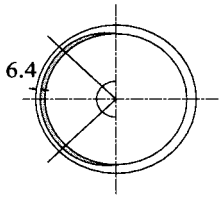

(c) 50% partial defect

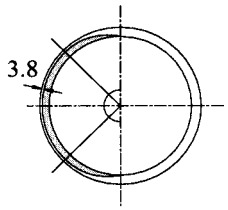

(d) 70% partial defect

(3) Wall thinning geometry at circumferential cross

Fig. 2 Elbow specimens with wall thinning. (1) Elbow specimen. (2) Longitudinal section. (3) Wall thinning geometry at circumferential cross: (a) No defect, (b) 50% full defect, (c) 50% partial defect, and (d) 70% partial defect.

thinning area for deep thinning pipe at the maximum moment. When a wall thinning area is subjected to compression stress, ovalization is generated for thin wall thinning pipe, or local buckling occurs for deep wall thinning pipe. The phenomenon of ovalization, crack initiation, or local buckling depends on the initial geometry of the wall thinning and the direction of the applied stress. Therefore, failure modes are summarized to be burst by internal pressure, ovailzation, crack, or local buckling by a monotonic bending load.

The failure mode for pipes receiving cyclic loading together with internal pressure is different from that receiving internal

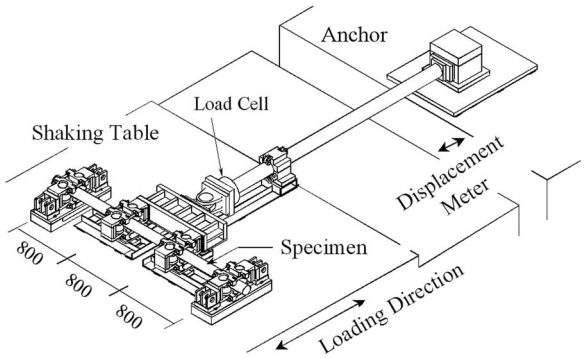

Fig. 3 Four-point bending test apparatus for straight pipe specimens

pressure or monotonic bending loading. The internal pressure during cyclic loading affects a deformation of the wall thinning pipe. The failure mode of cyclic loading with internal pressure accompanies swelling with ratchet for straight pipes (as shown in Table 4). Almost all failure modes are leakage by cracks accompanying swelling by ratchets. Other failure mode is a burst and crack with ratchet swelling for deep wall thinning pipe. Figure 6 is the ratchet deformation and burst by axial and circumferential cracks (EC07 specimen). Ratchet swelling always occurred for wall thinning pipes with constant internal pressure during cyclic loading.

Failure modes for elbow specimens were crack initiations/growths or crack initiation/growth after local buckling, as shown in Table 5. Figure 7 is the photograph of specimen ELBM-01. Local buckling occurred with ratchet deformation, and water that leaked from the crack penetrated the wall thickness.

Pressure blowout seems to be dependent on wall thinning depth, width, and length. An example of pressure blowout happened at the pressure of 2.5 MPa in a thermal power plant, as shown in Fig. 8. The outer diameter of the pipe was 318.5 mm, the nominal wall thickness was 10.3 mm, and the minimum required wall thickness by pressure was 4.15 mm. The remaining wall thickness around the burst hole was 1.0 mm. The remaining wall thickness was considerably thin compared with the minimum required wall thickness. Almost all specimens in the experiments did not show a pressure blowout such as in Fig. 8, under the condition of less than 75% wall thinning and thinning length of pipe diameter. It seems impossible to obtain pressure blowout during cyclic loading within this experimental condition. It is conceivable that pressure blowout might show deeper and longer wall thinning geometries. The features of fracture modes for wall thinning pipes under cyclic loading with constant internal pressure are combinations of crack growth and ratchet swelling.

Elastic Strain-Based Stress. To compare the experimental data with the design fatigue curve of ASME Code Sec. III [10], an amplitude of an elastic stress based on strain is needed. Design fatigue curves were determined from the best fit curves of data generated in the laboratory using polished round specimens by use of a safety factor of 2 on stress or of 20 on cycles, whichever is more conservative [11,12]. Although fatigue strengths in the high cyclic number areas were taken by specimens with stress controlled conditions, fatigue strengths at low cyclic number areas were taken by strain controlled specimens. The stresses in the low cyclic areas are evaluated by elastic strain-based stresses with the combination of strain and Young's modulus.

In the case of a straight pipe in these experiments, the elastic strain-based stress is calculated from a conversion of the load-line displacement. The elastic relation between the displacement at the load point and the reaction force R for four-point bending is given by

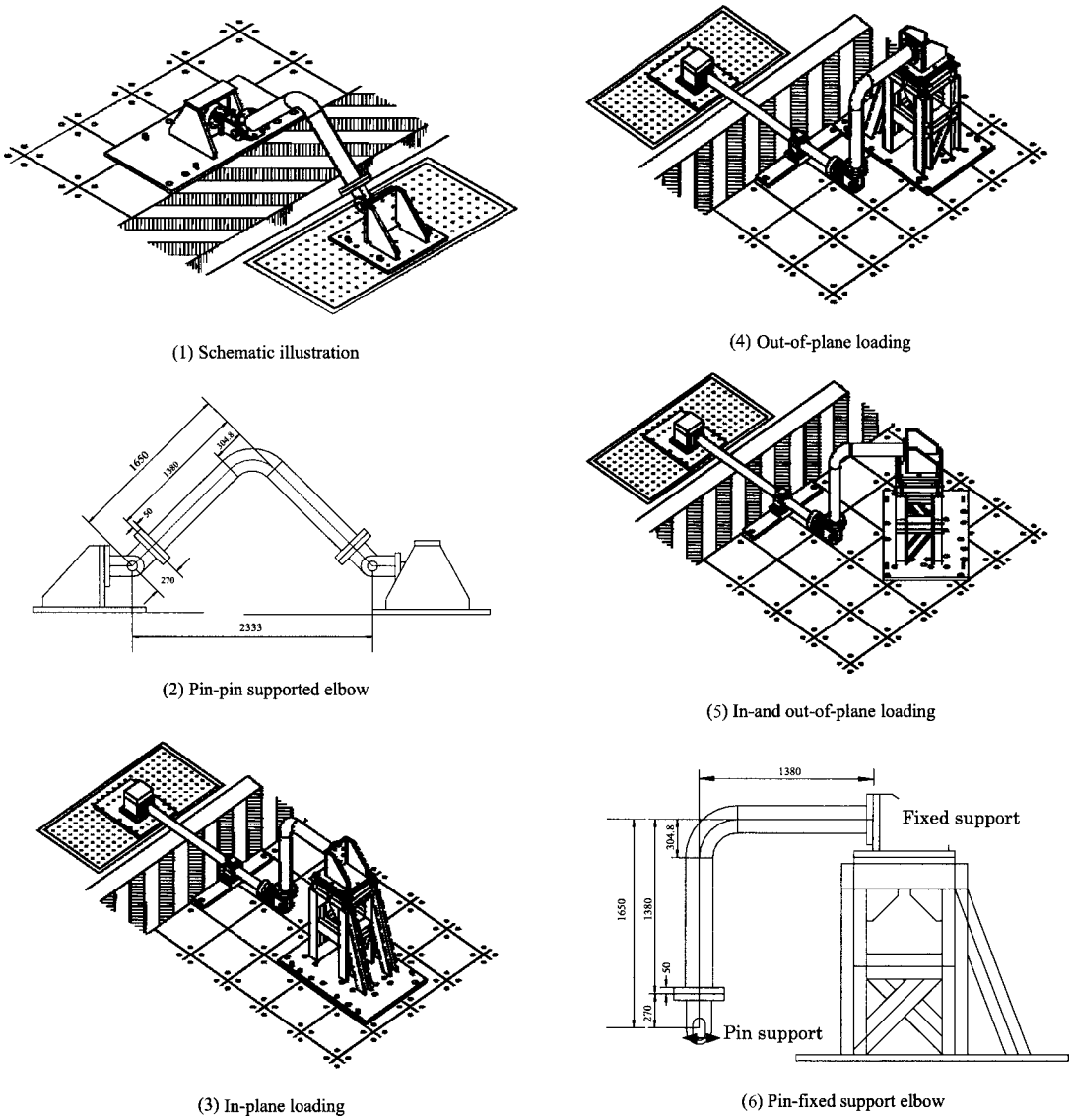

Fig. 4 (*a*) Test apparatus for elbow with in-plane cyclic bending load: (1) schematic illustration; (2) pin-pin supported elbow. (*b*) Test apparatus of pin-fixed support for elbow with cyclic bending load: (3) in-plane loading, (4) out-of-plane loading, (5) in- and out-of-plane loading, and (6) pin-fixed support elbow.

$$\delta = \frac{Rl_1^3}{6EI}\left(\frac{3l_2}{l_1} + 2\right) \tag{1}$$

where l_1 is the length of (major span–minor span)/2, l_2 the minor span length, E the Young's modulus, and I the moment of inertia. I for a cylinder is given by $I=\pi(D_2^4-D_1^4)/64$, where D_2 is the nominal outer diameter and D_1 is the nominal inner diameter of the cylinder. The reaction force is an elastic force based on displacement when the pipe deformation becomes plastic condition.

From the given δ, the elastic moment based on displacement M is obtained from the value of R as

$$M = Rl_2 \tag{2}$$

Therefore, the elastic strain-based stress for pipe bending is given by

$$\sigma_a = M/Z \tag{3}$$

where Z is the section modulus expressed by $Z=\pi(D_2^4-D_1^4)/(32D_2)$ for a cylinder. Then, an elastic strain-based stress for a straight pipe was obtained from the above relations, where nominal dimensions of $D_1=114.3$ mm and $D_2=97.1$ mm were used. The stress amplitude σ_a for wall thinned straight pipe specimens are shown in Table 4, together with the number of cycles to failure.

Table 4 also shows the applied stress σ_g, which is obtained from the actual reaction force R given by Table 2. It is understood that the elastic strain-based stress amplitude σ_a is greater than the applied stress σ_g at the plastic condition. The difference of stress σ_a minus stress σ_g increases with increasing wall thinning depth because the pipe with deep wall thinning can deform easily by a small applied load.

An elastic strain-based stress for an elbow specimen is not easy to obtain from an applied displacement. The sequence of the elastic strain-based stress calculation is shown in Fig. 9. Strain gages were put at the location of the straight pipe portion. Before the cyclic loading test with large displacement, strains at the location of C4-C4′ of the straight pipe portion were measured at an elastic range of small displacement, where C4-C4′ is the location of distance L_1 from the loading pin. From the strain distribution at the cross section of C4-C4′, the moment M_{C4} is calculated at a

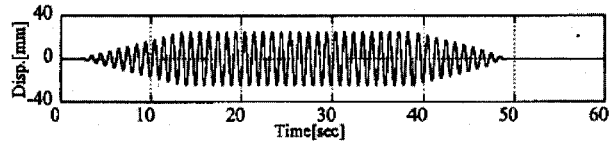

(1) Sinusoidal wave for straight pipe (One block is 26 cycles)

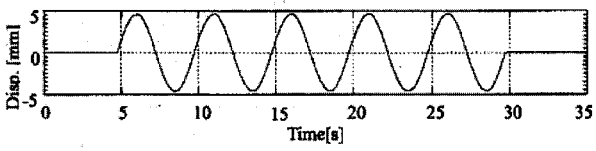

(2) Sinusoidal wave for elbow (One block is 5 cycles)

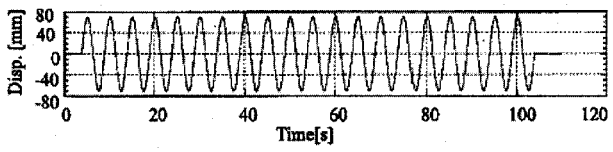

(3) Sinusoidal wave for elbow (One block is 20 cycles)

Fig. 5 Time histories of input displacement. (1) Sinusoidal wave for straight pipe (one block is 26 cycles). (2) Sinusoidal wave for elbow (one block is 5 cycles). (3) Sinusoidal wave for elbow (one block is 20 cycles).

given displacement. Using the moment M_{C4} at C4-C4′, the reaction force P at the loading pin is calculated from the distance L_1 between C4-C4′ and the pin. As the distance between the pin and the center of the elbow is L_2, the moment at elbow due to the displacement δ is

$$M = PL_2 \tag{4}$$

These moments with different elastic displacements were plotted in the moment-displacement curve in the elastic region. The intersection point of line extrapolated elastic region and the experimental displacement is the elastic strain-based moment. From the moment the elastic strain-based stress was obtained from $\sigma = M/Z$, where Z is the section modulus given by nominal pipe dimensions. The elastic strain-based stress amplitudes σ_a with the number of cycles to failure are shown in Table 5 for wall thinning elbow specimens.

Applied stresses σ_g for wall thinning elbows are shown in Table 5. The applied stresses were calculated from the maximum reaction moment based on the actual reaction force measured by the load cell. It is also understood that the elastic strain-based stress amplitudes σ_a is greater than the applied stresses σ_g.

Wall Thinned Pipes Under Seismic Events

The elastic strain-based stresses for straight pipes and elbows were derived from the displacement controlled cyclic tests, as mentioned above. Cumulative damages for the pipes and elbows are assessed by the elastic strain-based stresses and the number of cycles. Generally, to prevent the cumulative damage caused by many types of stress cycles such as startup-shutdown, turbine trips, seismic events, etc., piping items are designed by the usage factors obtained from the design fatigue curve defined by ASME Code Sec. III, shown in Fig. 10. The usage factor U is given by

$$U = \frac{n_1}{N_1} + \frac{n_2}{N_2} + \cdots < 1.0 \tag{5}$$

where n_i is the number of cycles at each type of stress cycle and N_i is the maximum number of each repetition, which would be allowable if this type of cycle was only one action. Equation (5) is called Miner's law. Cumulative usage factor U shall not exceed 1.0 as stipulated in NB-3222 of ASME Code Sec. III. If U is beyond 1.0, the piping system is redesigned to reduce the applied stresses.

The elastic strain-based stresses for the straight pipes and elbows used in this experiments can be compared with the low

Table 2 Test conditions of straight pipe specimens with 360 deg wall thinning

Spec. no.	Thinned depth d/t (%)	Internal pressure		Maximum displacement amplitude δ (mm)	Reaction force, $2R$ (kN)
		Pressure, p (MPa)	Axial stress σ_z (MPa)		
EC02	50	11	34	25	67.1
EC05	50	11	34	35	86.2
EC06	50	0	0	35	68.6
EC07	75	11	34	25	38.2
EC08	25	11	34	35	80.4
EC09	60	11	34	25	51.0

Table 3 Test conditions of elbow specimens with wall thinning

Spec. no.	Thinned depth, d/t (%)	Loading direction	Piping support	Internal pressure, p (MPa)	Input displacement, δ (mm)	Maximum reaction moment, M (kN m)
ELB01	No defect	In plane	Pin-Pin	10	70	146.1
ELB02	50 full			7	70	85.7
ELB03	50 part			10–7	70	102.8
ELB04	70 part			10	70	90.8
ELB05	50 full			10	70	78.4
ELBI-01	No defect	In plane	Pin-Fixed	10	185	134.2
ELBO-01	No defect	Out of		10	195	137.5
ELBO-02	50 full	plane		10	195	104.5
ELBM-01	50 full	In and out of plane		10	185	90.7

Table 4 Test results of straight pipe specimens with 360 deg wall thinning (Note: N_f = number of cycles, σ_g = applied stress, σ_a = elastic strain-based stress)

Spec. no.	Thinned depth, d/t (%)	N_f (cycles)	σ_g (MPa)	σ_a (MPa)	Failure mode
EC02	50	73	416	765	Crack with ratcheting
EC05	50	11	525	1071	Crack with ratcheting
EC06	50	9	391	1071	Crack after local buckling
EC07	75	9	251	756	Burst and crack with ratcheting
EC08	25	164	492	1071	Crack with ratcheting
EC09	60	22	324	765	Crack with ratcheting

cycle area of the design fatigue curve for carbon steel of ASME Code Sec. III. The design curves are applicable at a temperature not exceeding 371°C. The solid thin curve is for the steels with ultimate tensile strength (UTSs) of 791–895 MPa, while the solid thick curve is for the UTS smaller than 551 MPa.

The elastic strain-based stresses for straight pipes with wall thinning can be plotted on the design fatigue curve for carbon steel, as shown in Fig. 10. The experimental data are compared with the solid thick curve. When comparing the experimental data with the design fatigue curve, fatigue strength for the shallow depth of 25% wall thinning pipe (EC08) is located very close to the design curve. Cumulative damage determined by design stress is far less than the design fatigue curve. Therefore, wall thinning of 25% depth is said to be not a detrimental thinning.

The number of cycles in a seismic event for design is specific to the individual countries. The design number is assumed to be 60 cycles for light water reactors in Japan and about 10 cycles in the USA by the rule of USNRC (US Nuclear Regulatory Commission). At 60 cycles, the stress becomes 1700 MPa from the design fatigue curve. The stress of 1700 MPa is the maximum allowable stress for seismic events. However, alternating stresses are not only seismic stress but also other operational transient cycles. In addition, designs are generally endeavored to reduce the cumulative usage factors by installing piping supports, changing piping routes, etc. Applied stresses for seismic events are designed to be far bellow the stress of 1700 MPa.

Stresses cause by SSE in actual plants were surveyed at stress reports of ferritic piping systems. The maximum stress by SSE is about 122 MPa, which is determined from the acceleration of earthquake for piping items. The usage factor corresponding to 122 MPa is very small, that is, U = about 0.001. The maximum stress of 122 MPa is lined in Fig. 10. The area with N_f = 60 cycles and stress of 122 MPa is the actual maximum area of seismic regime by SSE.

When comparing the experimental data of straight pipes and seismic regime, all experimental data for straight pipes with local wall thinning are outside of the seismic regime. It is asserted from Fig. 10 that straight pipes with wall thinning does not break at SSE, even when the wall thinning depth is 75% of the nominal wall thickness.

Figure 11 shows the comparison of experimental data of elbows with wall thinning, seismic regime, and design fatigue curve. The experimental data are compared with the solid thick curve for the UTS smaller than 551 MPa. All data are plotted outside of the seismic regime of 10 cycles and 60 cycles.

Fatigue strengths for elbows under in-plane bending with pin-pin support or pin-fixed support have margins against SSE. However, numbers of failures for elbows (ELBO-02 and ELBM-01) under the out-of-plane or in- and out-of-plane conditions were relatively small. These elbow specimens receive bending stress at the end of the elbows and torsion stress at the other. In evaluating fatigue strength, torsion stresses are not included in the calculation of the elastic strain-based stress. In addition, elbows with no defects are also plotted in the lower side of the design curve. These data without defects shall be plotted above, at least on the design fatigue curve, because the design fatigue curve is determined by smooth specimens with a margin of 2 on stress and 20 on cycles. If more precise calculations for elastic strain-based stresses taking into account the torsion stresses are considered, the elastic strain-

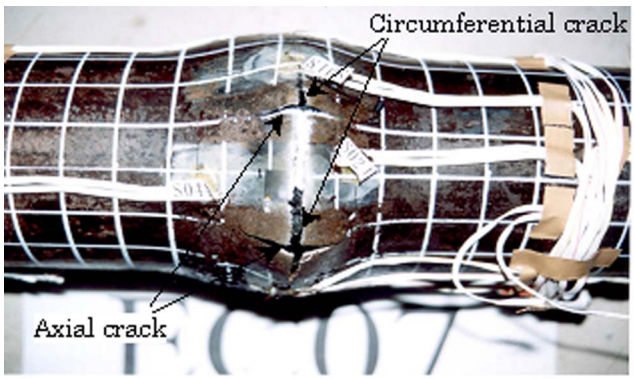

Fig. 6 Failure mode of the EC07 specimen

Table 5 Test results of elbow specimens with wall thinning (Note: N_f = number of cycles, σ_g = applied stress, σ_a = elastic strain-based stress)

Specimen no.	Thinned depth, d/t (%)	N_f (cycles)	σ_g (MPa)	σ_a (MPa)	Remarks
ELB01	No defect	179	347	597	Crack at flank with ratcheting
ELB02	50 full circumferential	319	218	316	Crack with ratchet after local buckling
ELB03	50 part	231	261	454	Crack at thinned flank with ratcheting
ELB04	70 part	177	233	413	Crack with ratcheting
ELB05	50 full circumferential	264	200	345	Crack with ratchet after local buckling
ELBI-01	No defect	110	343	773	Crack at flank with ratcheting
ELBO-01	No defect	>300	443	628	No failure
ELBO-02	50 full circumferential	40	269	525	Crack with ratchet after local buckling
ELBM-01	50 full circumferential	34	230	492	Crack with ratchet after local buckling

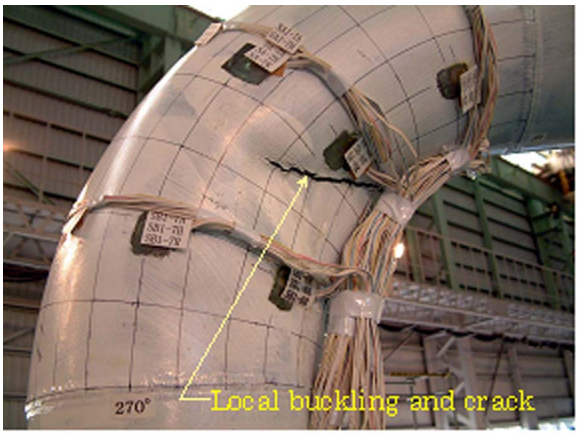

Fig. 7 Failure mode of the ELMB-01 specimen

based stresses would be larger and the experimental data of elbows of out-of-plane or in- and out-of-plane conditions will plotted more high stresses in Fig. 11.

The minimum required wall thickness t_{min} for a pipe defined by a construction code is determined based on a design internal pressure by a formula of $t_{min}=pD_2/(2S_m+0.8p)$, where p is the internal pressure and S_m is the design stress intensity. The design stress intensity for JIS STS 410 employed in this experiments is S_m =137 MPa at ambient temperature [13]. The minimum required

Fig. 8 Example of pressure blowout occurring at thermal power plant piping

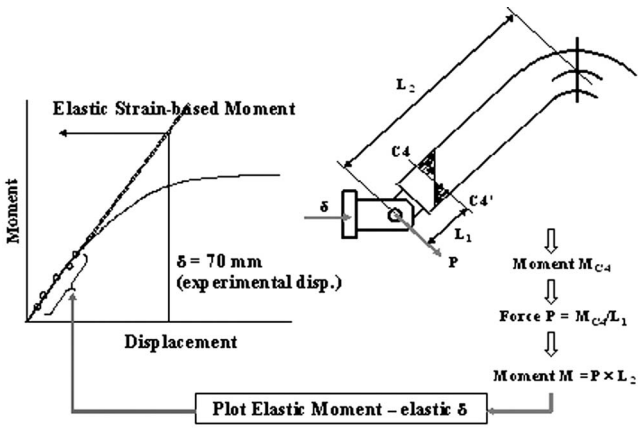

Fig. 9 Elastic strain-based moment for elbow

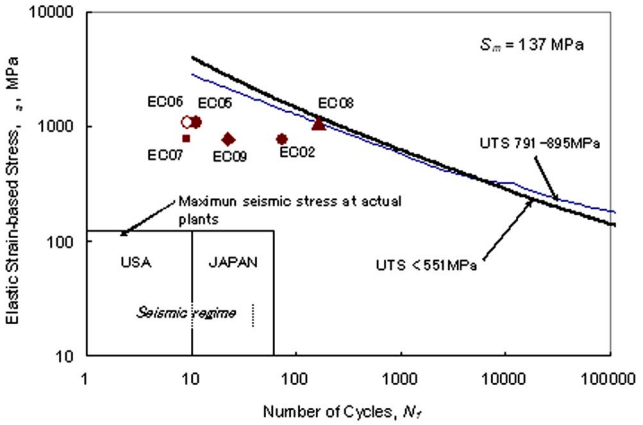

Fig. 10 Comparison of low cycle fatigue strengths for wall thinned straight pipes, seismic regime, and design fatigue curve

wall thickness t_{min} for the straight pipes under the pressure of 11 MPa are 52% of the nominal wall thickness, and t_{min} for the elbows under 10 MPa are 60% of the nominal wall thickness. The wall thinning of 50% or 70% for straight pipes and elbows used in these experiments is almost equal to or less than t_{min}. It is inferred thoroughly that, from Figs. 10 and 11, straight pipes and elbow pipes with less than the minimum required wall thickness do not break at SSE under the experimental conditions.

Conclusions

Cyclic loading experiments with or without internal pressure were performed on 4 in. diameter straight pipes and 8 in. diameter elbow pipes with wall thinning under displacement-controlled conditions at ambient temperature.

It is shown that almost all failure modes under cyclic loading for straight and elbow pipes were crack initiation and growth accompanying ratchet swelling or crack initiation and growth after local buckling. Another failure mode is a burst and crack with ratchet swelling for deep wall thinning pipes.

Low cycle fatigue strengths were compared with the seismic regime in the design fatigue curve defined by ASME Code Sec. III. The seismic regime that occurred at SSE has a maximum applied stress of 122 MPa and 60 cycles. It is concluded that from the comparison of the experimental data with the seismic regime, straight pipes and elbows with less than the minimum required wall thickness have sufficient margins against the seismic event of the SSE.

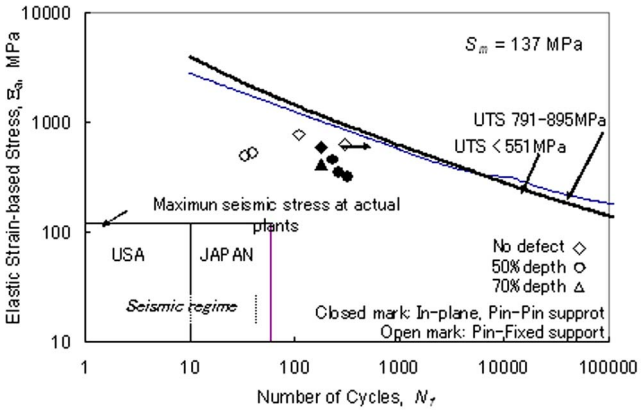

Fig. 11 Comparison of low cycle fatigue strengths for wall thinned elbows, seismic regime, and design fatigue curve

Acknowledgment

A part of this study was financially supported by the Budget for Nuclear Research of the Ministry of Education, Culture, Sports, Science and Technology based on the screening and counseling by the Atomic Energy Commission in Japan.

References

[1] The Japan Society of Mechanical Engineers, "Codes for Power Generation Facilities, Rules on Pipe Wall Thinning Management," JSME S CA1-2005, March 2005 (in Japanese).
[2] Isozaki, T., Shibata, K., Ueda, S., Kurihara, R., Onizawa, K., and Kohsaka, A., 1993, "Technical Report on the Piping Reliability Proving Tests at the Japan Atomic Energy Research Institute," Report No. JAERI-M 93-076.
[3] Miyazaki, K., Kanno, S., Ishiwata, M., Hasegawa, K., Ahn, S. H., and Ando, K., 1999, "Fracture Behavior of Carbon Steel Pipe With Local Wall Thinning Subjected to Bending Load," Nucl. Eng. Des., **191**, pp. 195–204.
[4] Ahn, S. H., Nam, K. W., Yoo, Y. S., Ando, K., Ji, S. H., Ishiwata, M., and Hasegawa, K., 2002, "Fracture Behavior of Straight Pipe and Elbow With Local Wall Thinning," Nucl. Eng. Des., **211**, pp. 91–103.
[5] Hasegawa, K., Sakata, K., Miyazaki, K., and Kanno, S., 2002, "Fatigue Strength for Pipes With Allowable Flaws and Design Fatigue Curve," Int. J. Pressure Vessels Piping, **79**, pp. 37–44.
[6] Shin, D. J., Choi, J. B., and Kim, Y. J., 2004, "Failure Strength Assessment of Pipes With Local Wall Thinning Under Combined Loading Based on Finite Element Analyses," ASME J. Pressure Vessel Technol., **126**, pp. 179–183.
[7] Kim, Y. J., Shim, D. J., Lim, H., and Kin, Y. J., 2004, "Reference Stress Based on Approach to Predict Failure Strength of Pipes With Local Wall Thinning Under Single Loading," ASME J. Pressure Vessel Technol., **126**, pp. 194–201.
[8] Hasegawa, K., Wilkowski, G., Goyette, L., and Scarth, D., 2004, "Development of Analytical Evaluation Procedures and Acceptance Criteria for Pipe Wall Thinning in ASME Code Section XI," *Proceedings of 2004 ASME Pressure Vessels and Piping Conference*, San Diego, Vol. 474, pp. 83–88.
[9] Nakamura, I., 2004, "Study on Damage Behavior and Evaluation at Seismic Events for Degraded Piping (in Japanese)," Ph.D. thesis, Yokohama National University.
[10] 2004, ASME P&PV Code Sec. III, Div. I, Appendix 1.
[11] ASME, 1969, *Criteria of the ASME Boiler and Pressure Vessel Code for Design by Analysis in Section III and VIII, Division 2*, ASME, New York.
[12] ASME, 1972, *Pressure Vessels and Piping: Design and Analysis: A Decade of Progress*, ASME, New York, Vol. 1.
[13] The Japan Society of Mechanical Engineers, 2005, "Codes for Nuclear Power Generation Facilities, Rules on Design and Construction for Nuclear Power Plants," Report No. JSME S NC1-2005.